NANO LETTERS

pubs.acs.org/NanoLett

Double-Gate Nanowire Field Effect Transistor for a Biosensor

Jae-Hyuk Ahn,[†,⊥] Sung-Jin Choi,[†,⊥] Jin-Woo Han,[†,⊥] Tae Jung Park,[‡,⊥] Sang Yup Lee[‡,§,||,⊥] and Yang-Kyu Choi*[,†,§]

[†]Department of Electrical Engineering, [‡]BioProcess Engineering Research Center, Center for Systems and Synthetic Biotechnology, and Institute for the BioCentury, [§]Department of Chemical and Biomolecular Engineering, and [||]Department of Biological Sciences, Department of Bio and Brain Engineering, and Bioinformatics Research Center, KAIST, 335 Gwahangno, Yuseong-gu, Daejeon 305-701, Republic of Korea

ABSTRACT A silicon nanowire field effect transistor (FET) straddled by the double-gate was demonstrated for biosensor application. The separated double-gates, G1 (primary) and G2 (secondary), allow independent voltage control to modulate channel potential. Therefore, the detection sensitivity was enhanced by the use of G2. By applying weakly positive bias to G2, the sensing window was significantly broadened compared to the case of employing G1 only, which is nominally used in conventional nanowire FET-based biosensors. The charge effect arising from biomolecules was also analyzed. Double-gate nanowire FET can pave the way for an electrically working biosensor without a labeling process.

KEYWORDS Double-gate, nanowire, field effect transistor, FinFET, biosensor, sensitivity, avian influenza (AI)

Semiconductor nanowires have great potential in the direct electrical detection of biomolecules due to their high sensitivity.[1−3] Charged molecules on nanowire surfaces induce a field gating effect that changes the current or its corresponding conductance through the nanowire. In principle, this effect is strong enough to detect single charges.[4,5] In most reports, nanowire biosensors were fabricated by the use of bottom-up approaches because of their attractiveness in controlling a nanometer-sized feature.[6−9] These approaches, however, have a few weaknesses in position and shape control because they rely on a random process. Moreover, integrability can be a serious concern. Compatibility with the standard complementary metal oxide semiconductor (CMOS) process is highly attractive for implementation of the readout and signal control circuit onto the same substrate in terms of monolithic integration. On the contrary, top-down approaches can utilize a well-established CMOS technology,[10−12] thereby overcoming the aforementioned difficulties, reducing the cost, and improving the reliability. To achieve high sensitivity, researchers have made attempts to scale down a structural dimension of the nanowires, including width[4,12] and thickness.[13] But the top-down approaches inevitably impose a constraint in delineating ultrasmall feature sizes for high sensitivity and increasing throughput for cost reduction in the case of electron beam (e-beam) lithography or size reduction by employment of iterative oxidation, and removal of its oxide may be indispensable; hence, the fabrication process becomes unwontedly complicated. Thus, it is important to find a new alternative in a structural point of view while we keep completely utilizing the CMOS compatibility neither usage of advanced lithographic tools nor employment of the size reduction technique.

Herein, we propose a double-gate nanowire FET biosensor, which has separated double-gates, that is, G1 and G2, that sit vertically on the silicon nanowire and face each other, as shown in Figure 1. It is noteworthy that the aggressively scaled dimensions of the silicon nanowire are not necessary in this approach. By comparison with conventional nanowire FET biosensor activated by a single back-gate (or bottom gate), the most remarkable difference in the double-gate FET is that symmetric/asymmetric biases can be applied to two gates. A conduction path in the silicon nanowire is controlled independently and precisely. Thus, sensitivity is improved compared to an operational scheme with a single gate only, especially in the subthreshold regime, which is an optimal

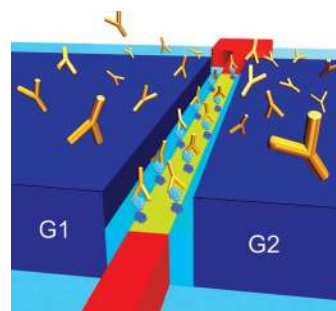

FIGURE 1. Schematic of the double-gate nanowire FET with immobilized biomolecules. Anti-AI (antibodies, Y-shape) are diffused through a solution and selectively bound to its antigens, which are immobilized onto the opened channel at the top of the nanowire.

* To whom correspondence should be addressed. E-mail: ykchoi@ee.kaist.ac.kr.
[⊥] E-mail adresses: (J.-H.A.) jhahn@nobelab.kaist.ac.kr; (S.-J.C.) sjchoi@nobelab.kaist.ac.kr; (J.-W.H.) jinu0707@nobelab.kaist.ac.kr; (T.J.P.) tjpark@kaist.ac.kr; (S.Y.L.) leesy@kaist.ac.kr.
Received for review: 03/29/2010
Published on Web: 07/12/2010

© 2010 American Chemical Society

DOI: 10.1021/nl1010965 | *Nano Lett.* **2010,** *10,* 2934–2938

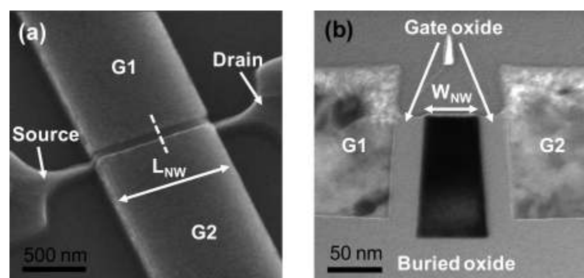

FIGURE 2. Images of the fabricated double-gate nanowire FET. (a) SEM image from a bird's eye view, showing gate 1 (G1) and gate 2 (G2), which contact both sides of the nanowire. (b) Cross-sectional TEM image along the dashed line in (a). G1 and G2 are physically separated by the gate and buried oxide.

sensing domain.[14] This suggested structure is very similar to the double-gate FinFET[15] except for the separated gate by a chemical–mechanical polishing (CMP) process. It should be noted that the FinFETs have nearly been commercialized because it has matured as a technology. There is no risk to employ such matured technology for nanowire FET-based biosensor application.

Double-gate nanowire FETs were fabricated by the use of an 8 in. silicon-on-insulator (SOI) wafer (see the Supporting Information, Figure S1). The wafer has a top Si thickness of 100 nm, which was initially doped with boron and measured with a resistivity of 9 to 18 $\Omega \cdot$cm, that is, an approximate doping concentration of 10^{15} cm^{-3}. Underneath this Si, there is the buried oxide with a thickness of 140 nm. As a first step, nitride 50 nm thick was deposited for etch stopper during the subsequent CMP process to separate the gate. The widths of nanowires range from 50 to 110 nm, which were patterned by the use of optical lithography with 193 nm wavelength from KrF and conventional plasma etching. Afterward, tetraethyl orthosilicate (TEOS) oxide 30 nm thick and n+ in situ doped polycrystalline silicon (poly-Si) 110 nm thick were deposited for a gate dielectric and a gate electrode, respectively. By employment of the CMP process, the protruded poly-Si on the nanowire channel begins to be polished and is then completely removed so that the connected single gate is separated into the double-gate. After patterning a gate region, the source and drain electrodes were formed by the use of arsenic implantation with 30 keV of energy and a dose of 5×10^{15} cm^{-2}. The etch stopper nitride was removed by hot phosphoric acid. To cure damage stemming from the nitride etching process on the top surface of the nanowire, additional oxidation was carried out to grow a 3 nm thermal oxide at 700 °C for 30 min in an oxygen ambient.

Figure 2a shows a bird's eye view of a scanning electron microscope (SEM) image of the fabricated double-gate nanowire FET. The two gates are straddling both sidewalls of the nanowire. Drain current (I_D), flowing from the drain to grounded source, was modulated by both or either of G1 and G2. G1 was assigned as a primary gate, and G2 was set as a

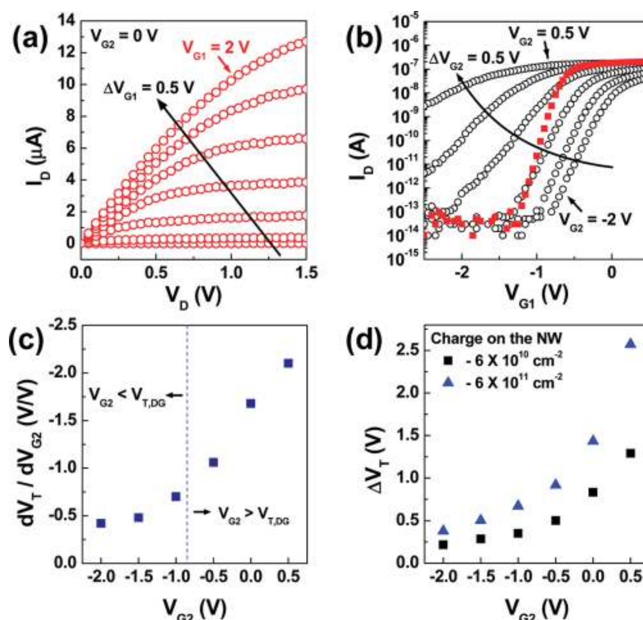

FIGURE 3. Measured $I-V$ characteristics of the double-gate nanowire FET of 110 nm width (W_{NW}) and 1 μm length (L_{NW}). (a) I_D-V_D characteristics for a V_{G1} of -1.0 to 2.0 V with a stepsize of 0.5 V and at $V_{G2} = 0$ V. (b) I_D-V_{G1} characteristics for V_{G2} of -2.0 to 0.5 V with a stepsize of 0.5 V and $V_D = 50$ mV. DG mode with $V_{G1} = V_{G2}$ is denoted by red squares. (c) dV_T/dV_{G2} extracted from the I_D-V_{G1} characteristics in (b) versus V_{G2}. In the $V_{G2} > V_{T,DG}$ (threshold voltage in DG mode), the device shows a much larger V_T shift as the V_{G2} changes. (d) Simulated V_T shift versus V_{G2}. V_T shift is calculated after the injection of charges with a value of -6×10^{10} (black squares) and -6×10^{11} cm^{-2} (blue triangles) on the top of the nanowire. When V_{G2} increases, the device shows a much larger V_T shift, which is a response to the charges.

secondary gate. Reversed roles of G1 and G2 can definitely work due to the symmetric structure of the two gates. Figure 2b shows a cross-sectional transmission electron microscope (TEM) image that was taken along the dashed line of G1-nanowire-G2 depicted in Figure 2a. G1 and G2 were physically isolated from the nanowire by virtue of the gate- and buried-oxide. Biomolecules were immobilized onto the opened channel at the top of the nanowire, as shown in Figure 1. Their intrinsic charges from the biomolecules directly affect the channel potential; hence, the current–voltage ($I-V$) characteristics are modulated accordingly.

To characterize the fabricated double-gate nanowire FETs, a semiconductor parameter analyzer (HP 4156C) was used. As shown in Figure 3a, the FETs show the typical $I-V$ characteristics of conventional n-channel metal oxide semiconductor field effect transistors (n-MOSFETs). When the G1 voltage (V_G) is larger than the threshold voltage (V_T), it induces inversion electrons and the drain current starts to flow. As we pointed out, there are two ways to drive the MOSFET in the double-gate structure, that is, single-gate (SG) mode and double-gate (DG) mode.[16] In SG mode, G1 is used as a drive gate and G2 serves as a supplementary gate to pin the channel potential at a fixed voltage. The role of G2 is analogous to that of the body terminal in the standard

© 2010 American Chemical Society

DOI: 10.1021/nl1010965 | Nano Lett. 2010, 10, 2934–2938

4-terminal MOSFET. In contrast, G1 and G2 are connected in DG mode, which implies that the same voltage is always applied to G1 and G2. Data measured in the SG mode (hollow circles) in Figure 3b show that current controllability by G1 can be changed according to the bias condition of G2, as was done by the back body bias in the standard MOSFET. In the n-channel MOSFET, the increment of the G2 voltage (V_{G2}) from negative to positive value tends to lower V_T and degrades the subthreshold slope (SS), defined as d(V_{G1})/d(log I_D), that is, it becomes less steep. However, the characteristics of DG mode (red squares) show steeper SS than that of SG mode due to the nature of the double-gate. As shown in Figure 3c, when V_{G2} is larger than $V_{T,DG}$ (V_T in the DG mode), V_T significantly changes in response to a small change of V_{G2}, which means it is very sensitive to V_{G2}. Comparatively, changes in V_T are independent of V_{G2} when V_{G2} is less than $V_{T,DG}$. From these properties of the double-gate nanowire FETs, it is inferred that the double-gate nanowire FET under a condition of $V_{G2} > V_{T,DG}$ is more effectively influenced by the extra charged biomolecules than the single-gate nanowire FET; thereafter, improved sensitivity is expected in the double-gate nanowire FET. To confirm G2's influence on sensitivity, a numerical simulation was performed using a three-dimensional semiconductor simulation package (ATLAS in SILVACO Inc.).[17] The extra charge, a role of charged biomolecules bound on top of the silicon nanowire, was set to a value of -6×10^{10} cm^{-2} (black squares in Figure 3d) and -6×10^{11} cm^{-2} (blue triangles in Figure 3d), respectively. Figure 3d shows that V_T shift (ΔV_T), due to the introduction of the charges, is enhanced when G2 is at positive bias, which corresponds to a condition of $V_{G2} > V_{T,DG}$. It is noteworthy that the differing values of ΔV_T between the cases setting a charge with -6×10^{10} and -6×10^{11} cm^{-2} increases as V_{G2} increases, which means that the signal resolution to distinguish different concentrations of target biomolecules can be improved.

As shown in Figure 4, negatively charged species, that is, antibodies, bound to antigens immobilized on the top of the nanowire take the inversion layer (electron channel) away from the top; hence, the current is reduced (see the Supporting Information, Figure S2). ΔV_T is extracted from the I_D-V_{G1} plot at the fixed drain current (I_D) between the time before and after immobilization of the biomolecules. As shown in Figure 4a, since the electron channel is formed close to the G1 side under the condition of $V_{G2} < V_{T,DG}$, G1 can control the channel efficiently; hence, it leads to small ΔV_T in the subthreshold region. Under the condition of $V_{G2} > V_{T,DG}$, shown in Figure 4b, however, the channel is far from the G1 side; hence, G1 loses the controllability of the channel potential. As a result, ΔV_T starts to increase.

To verify the aforementioned benefit in the double-gate nanowire FET, that is, the impact of G2 on sensitivity, bioexperiments using the specific antigen–antibody interaction for the detection of the avian influenza (AI) virus were carried out.[18−20] AI antigen (AIa) fused with silica-binding protein (SBP) was immobilized on the top surface of the nanowire via SBP domain, which plays the role of an anchor (Figure 1). A drop of 100 μL of SBP-AIa dissolved in 25 μg/mL (86.7 nmol/L SBP-AIa) of phosphate-buffered saline (PBS, pH 7.4) solution was cast on the double-gate nanowire device for 1 h at room temperature. Then, it was rinsed several times with deionized water and was subsequently dried with N_2 gas. Anti-AI antibody dissolved in 20 μg/mL (133.6 nmol/L anti-AI) of PBS solution was introduced on the SBP-AIa-immobilized device in the same way; hence, the specific binding between SBP-AIa and anti-AI was accomplished. The anti-AI was successfully detected up to concentration of 200 ng/mL (1.34 nmol/L anti-AI) (see the Supporting Information, Figure S3). Figure 5a−c shows I_D-V_{G1} characteristics before and after anti-AI binding in the same device for various V_{G2}, including the floating G2 condition, which is very similar to conventional single-gate nanowire FET without G2. Inherent negative charges of anti-AI increase V_T and, resultantly, decrease I_D in the n-channel MOSFET.[19] This unique property of V_T and I_D depending on charge polarity was verified by the use of 34-mer single-stranded DNA (ssDNA) of 10 nmoles to show negative charges that were immobilized with the aid of positively charged 3-aminopropyltriethoxysilane (APTES), which served as a self-assembled monolayer (SAM) (see the Supporting Information, Figure S4). I_D was increased with the reduced V_T due to positive charges stemming from APTES modification. However, I_D was decreased again after ssDNA absorption by the negative charges, which led to an increment of V_T. This verifies that the double-gate nanowire FET can

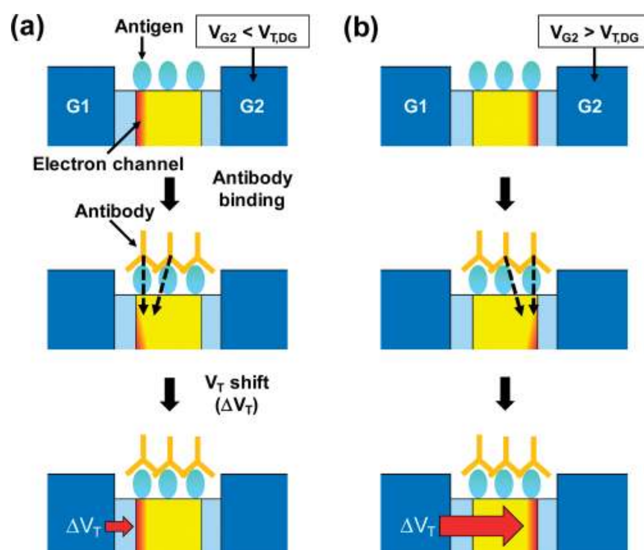

FIGURE 4. The effect of V_{G2} conditions on the V_T shift. Negatively charged antibodies take an electron channel away from the top. (a) $V_{G2} < V_{T,DG}$. Since the formed channel is close to the G1 side, G1 can easily control the channel, leading to a small V_T shift. (b) $V_{G2} > V_{T,DG}$. The channel is induced on the G2 side. The V_T shift increases due to the relatively large distance between G1 and the formed channel.

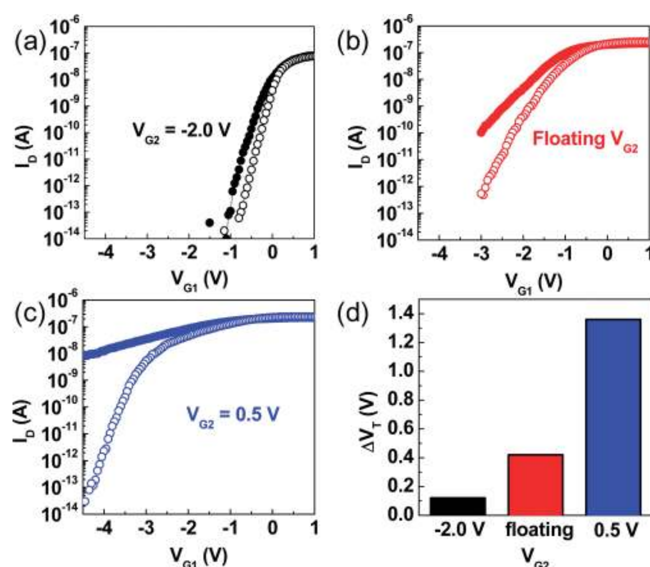

FIGURE 5. Measured I_D-V_{G1} characteristics by the change of the V_{G2} condition of the double-gate nanowire FET 110 nm in width (W_{NW}) and 1 μm in length (L_{NW}). Antigen of avian influenza (AIa) fused with the silica-binding protein (SBP) was first immobilized (filled circle), and afterward anti-AI was specifically bound with AIa (hollow circle). The concentration of SBP-AIa and anti-AI are 25 μg/mL (86.7 nmol/L) and 20 μg/mL (133.6 nmol/L), respectively. (a) $V_{G2}= -2.0$ V ($<V_{T,DG}$). (b) Floating G2 in which the device has the same configuration as a conventional single-gate FET. (c) $V_{G2} = 0.5$ V ($>V_{T,DG}$). (d) V_T shift extracted from the I_D-V_{G1} characteristics in (a−c) plotted versus various V_{G2} conditions.

electrically detect negatively charged anti-AI without a labeling process or an extra transducer to transform the measured signals.

V_{G2} is applied in the following three cases: (1) SG mode with $V_{G2} < V_{T,DG}$, (2) SG mode with floating V_{G2}, and (3) SG mode where $V_{G2} > V_{T,DG}$. When V_{G2} of -2.0 V ($<V_{T,DG}$) is applied, there is no remarkable change in the SS, V_T, or I_D, as shown in Figure 5a. On the contrary, as shown in Figure 5c, the SS, V_T, and I_D are dramatically changed when a V_{G2} of 0.5 V ($>V_{T,DG}$) was used. It is noteworthy that this bias condition shows enhanced sensitivity compared to case (2), which is the most similar to a conventional single-gate nanowire FET, as shown in Figure 5b. Similarly, ΔV_T in Figure 5d is extracted by employment of the constant current method, i.e. the referenced V_T in the V_{G1} scale was read at I_D of 10 nA. It is concluded that the best sensitivity was found at the condition of $V_{G2} > V_{T,DG}$. Therefore, the double-gate nanowire FET with the supportive gate (G2) enhances sensitivity more than the single gate nanowire FET even for the same dimensions of nanowire and fixed concentration of biomolecules.

In summary, the label-free electrical detection of biomolecules by the double-gate nanowire FETs was demonstrated. The proposed FETs are composed of two gates, primary and secondary, in an electrical way but the same gate in a physical way, and these gates were vertically straddling on the silicon nanowire. By means of the secondary gate, it is easy to control the carrier conduction paths, which critically affect the device parameters such as the subthreshold slope, threshold voltage, and drain current. It was experimentally observed by antibody−antigen interaction and theoretically supported by the commercialized simulator that the nanowire structure with the double gate showed improved sensitivity compared to that with a conventional single gate. Moreover, the charge effect of biomolecules was investigated by use of the negative charge of both antibodies from avian influenza and DNA. Since sensitivity enhancement becomes obscure only when scaling down the nanowire size, it is the right time to find a new approach by implementation of a double gate and utilization of the full advantages of matured CMOS technology.

Acknowledgment. This research was supported by Grant 08K1401-00210 from the Center for Nanoscale Mechatronics and Manufacturing, one of the 21st Century Frontier Research Programs supported by the Korea Ministry of Education, Science and Technology (MEST). It was also supported by the National Research and Development Program (Grant 2009-0065615) for the development of biomedical function monitoring biosensors, and the National Research Foundation of Korea funded by the Korean government (Grant 2009-0083079).

Supporting Information Available. Detailed fabrication process of double-gate nanowire FETs, an experimental section describing a response of double-gate nanowire FETs depending on charge polarity and simulation of electron density after charged species binding. This material is available free of charge via the Internet at http://pubs.acs.org.

REFERENCES AND NOTES

(1) Cui, Y.; Wei, Q.; Park, H.; Lieber, C. M. *Science* **2001**, *293*, 1289–1292.
(2) Zheng, G.; Patolsky, F.; Cui, Y.; Wang, W. U.; Lieber, C. M. *Nat. Biotechnol.* **2005**, *23*, 1294–1301.
(3) Li, Z.; Chen, Y.; Kamins, T. I.; Nauka, K.; Williams, R. S. *Nano Lett.* **2004**, *4*, 245–247.
(4) Elfström, N.; Juhasz, R.; Sychugov, I.; Engfeldt, T.; Eriksson Karlström, A.; Linnros, J. *Nano Lett.* **2007**, *7*, 2608–2612.
(5) Patolsky, F.; Zheng, G.; Hayden, O.; Lakadamyali, M.; Zhuang, X.; Lieber, C. M. *Proc. Natl. Acad. Sci. U.S.A.* **2004**, *101*, 14017–14022.
(6) Li, C.; Curreli, M.; Lin, H.; Lei, B.; Ishikawa, F. N.; Datar, R.; Cote, R. J.; Thompson, M. E.; Zhou, C. *J. Am. Chem. Soc.* **2005**, *127*, 12484–12485.
(7) Shao, M.-W.; Shan, Y.-Y.; Wong, N.-B.; Lee, S.-T. *Adv. Funct. Mater.* **2005**, *15*, 1478–1482.
(8) Shan, Y.; Kaan Kalkan, A.; Peng, C.-Y.; Fonash, S. J. *Nano Lett.* **2004**, *4*, 2085–2089.
(9) Whang, D.; Jin, S.; Wu, Y.; Lieber, C. M. *Nano Lett.* **2003**, *3*, 1255–1259.
(10) Stern, E.; Klemic, J. F.; Routenberg, D. A.; Wyrembak, P. N.; Turner-Evans, D. B.; Hamilton, A. D.; LaVan, D. A.; Fahmy, T. M.; Reed, M. A. *Nature* **2007**, *445*, 519–522.
(11) Gao, Z.; Agarwal, A.; Trigg, A. D.; Singh, N.; Fang, C.; Tung, C.-H.; Fan, Y.; Buddharaju, K. D.; Kong, J. *Anal. Chem.* **2007**, *79*, 3291–3297.

(12) Kim, A.; Ah, C. S.; Yu, H. Y.; Yang, J.-H.; Baek, I.-B.; Ahn, C.-G.; Park, C. W.; Jun, M. S. *Appl. Phys. Lett.* **2007**, *91*, 103901.
(13) Elfström, N.; Eriksson Karlström, A.; Linnros, J. *Nano Lett.* **2008**, *8*, 945–949.
(14) Gao, X. P. A.; Zheng, G.; Lieber, C. M. *Nano Lett.* **2010**, *10*, 547–552.
(15) Choi, Y.-K.; King, T.-J.; Hu, C. *IEEE Electron Device Lett.* **2002**, *23*, 25–27.
(16) Masahara, M.; Liu, Y.; Sakamoto, K.; Endo, K.; Matsukawa, T.; Ishii, K.; Sekigawa, T.; Yamauchi, H.; Tanoue, H.; Kanemaru, S.; Koike, H.; Suzuki, E. *IEEE Trans. Electron Device* **2005**, *52*, 2046–2053.
(17) *ATLAS User's Manual*; SILVACO Inc.: Santa Clara, CA 2008.
(18) Gu, B.; Park, T. J.; Ahn, J.-H.; Huang, X.-J.; Lee, S. Y.; Choi, Y.-K. *Small* **2009**, *5*, 2407–2412.
(19) Kim, S.; Ahn, J.-H.; Park, T. J.; Lee, S. Y.; Choi, Y.-K. *Appl. Phys. Lett.* **2009**, *94*, 243903.
(20) Lee, K.-W.; Choi, S.-J.; Ahn, J.-H.; Moon, D.-I.; Park, T. J.; Lee, S. Y.; Choi, Y.-K. *Appl. Phys. Lett.* **2010**, *96,* 033703.

© 2010 American Chemical Society

DOI: 10.1021/nl1010965 | *Nano Lett.* **2010,** *10,* 2934--2938